ACS APPLIED MATERIALS & INTERFACES

Research Article

www.acsami.org

Investigation of the Electric Structures of Heterointerfaces in Pt- and In_2S_3-Modified $CuInS_2$ Photocathodes Used for Sunlight-Induced Hydrogen Evolution

Gunawan,[†,‡] Wilman Septina,[†] Takashi Harada,[†] Yoshitaro Nose,[§] and Shigeru Ikeda*[,†]

[†]Research Center for Solar Energy Chemistry, Osaka University, 1-3 Machikaneyama, Toyonaka, Osaka 560-8531, Japan

[‡]Chemistry Department, Faculty of Science and Mathematics, Diponegoro University, Semarang, Indonesia

[§]Department of Materials Science and Engineering, Kyoto University, Yoshida-Honmachi, Sakyo-ku, 606-8501 Kyoto, Japan

Supporting Information

ABSTRACT: Copper indium disulfide ($CuInS_2$) modified with an In_2S_3 layer and a Pt catalyst showed a more efficient photoelectrochemical (PEC) property for hydrogen evolution from a nearly neutral (pH 6) 0.2 M NaH_2PO_4 solution under simulated sunlight illumination (AM 1.5G) than that of a $CuInS_2$ electrode modified with a CdS layer and a Pt catalyst. Analysis of the PEC properties of In_2S_3-modified $CuInS_2$ ($In_2S_3/CuInS_2$) and CdS-modified $CuInS_2$ ($CdS/CuInS_2$) in solutions containing an electron scavenger (Eu^{3+}) showed identical enhancement of the PEC properties of $In_2S_3/CuInS_2$ when compared to those of $CdS/CuInS_2$, indicating the formation of a favorable heterointerface in $In_2S_3/CuInS_2$ for efficient charge separation. Spectroscopic evaluation of conduction band offsets revealed that $In_2S_3/CuInS_2$ had a notch-type conduction band offset, whereas a cliff-type offset was formed in $CdS/CuInS_2$: these results also revealed a better interface electric structure of $In_2S_3/CuInS_2$ than that of $CdS/CuInS_2$.

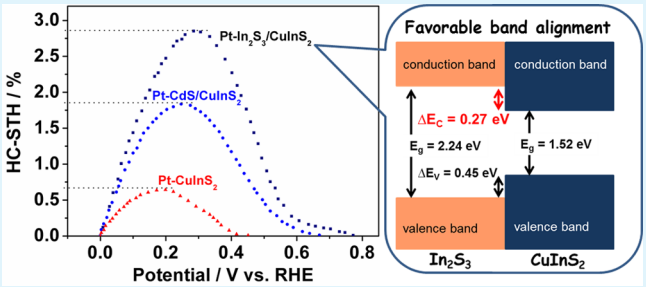

KEYWORDS: *photocathodes, copper indium disulfide, indium disulfide, heterointerface, X-ray photoelectron spectroscopy*

1. INTRODUCTION

Hydrogen (H_2) production by photoelectrochemical (PEC) splitting of water via direct use of sunlight irradiation is considered to be an ideal pathway to provide sustainable fuel that can support human life for many years to come. This idea has motivated the scientific community to develop such a system by exploring various materials and strategies. Fujishima et al. demonstrated the first realization of water splitting via the PEC approach by using a TiO_2 photoelectrode illuminated with UV light under application of a bias energy.[1] Since then, numerous varieties of semiconductors and device configurations have been investigated to realize an efficient water splitting system for producing H_2.[2−6]

Due to the difficulty in finding a single semiconductor that is able to efficiently perform both water reduction and oxidation simultaneously, a tandem water splitting system has emerged as the most viable solution for practical application. This system consists of a photocathode and a photoanode that are responsible for water reduction and oxidation, respectively. This system allows flexibility in investigating and optimizing a potential semiconductor for each of the electrodes, which is promising to achieve an efficient overall water splitting system using only sunlight without the requirement of any bias energy.

With regard to the photocathode part, Cu-chalcopyrite materials such as $CuInSe_2$, $CuGaSe_2$, $CuInS_2$, $CuGaS_2$, and their mixed crystals have emerged as promising candidates for a high-performance H_2 evolutor.[7−13] Moreover, tunable band gap values (1.0−2.4 eV) by changing the In/Ga and/or Se/S ratios in their mixed crystal are promising for versatile flexibility in optimizing the appropriate design in tandem with the photoanode part. Insertion of n-type thin layers on photocathodes to improve the photoresponse had been done by researchers using different absorbers, which are widely employed to fabricate p−n junctions for chalcopyrite-based solar cells.[12−17] In our previous study, we used In_2S_3 by chemical bath deposition (CBD) as an alternative to the commonly used CdS as the n-type layer on a $CuInS_2$ photocathode, and the use of In_2S_3 resulted in half-cell solar-to-hydrogen (HC-STH) efficiency close to 2%.[12] Furthermore, the onset of the photocurrent was shifted positively, which made this photocathode system more favorable for a tandem PEC system without any bias voltage.

Although an In_2S_3-modified $CuInS_2$ photocathode showed higher water reduction properties than those of the CdS-modified one and is a promising photocathode for a tandem water splitting system, the reason for this superiority has remained unclear. This motivated us to study the properties of these junctions. In this study, therefore, the reason for the

Received: May 27, 2015
Accepted: July 2, 2015
Published: July 2, 2015

DOI: 10.1021/acsami.5b04634
ACS Appl. Mater. Interfaces 2015, 7, 16086−16092

superiority of In_2S_3-modified $CuInS_2$ to CdS-modified $CuInS_2$ was investigated with focusing on the electric structures of those heterointerfaces.

2. EXPERIMENTAL SECTION

Fabrication of $CuInS_2$ Thin Films. A $CuInS_2$ thin film was synthesized by electrodeposition of Cu and In layers followed by sulfurization. Electrodeposition was carried out potentiostatically using a Hokuto Denko HSV-100 potentiostat-galvanostat under an N_2 atmosphere without stirring. A vertical three-electrode setup consisting of an Ag/AgCl reference electrode, a Pt wire counter electrode, and an Mo-coated glass substrate (Mo/glass) as a working electrode (area of the working electrode being 0.7 cm^2) was employed. The electrolyte solution for the Cu deposition consisted of 50 mM $CuSO_4$, 150 mM trisodium citrate, and 242 mM citric acid. The solution was adjusted to pH 2.4 using H_2SO_4. For In deposition, an aqueous solution containing 30 mM $InCl_3$, 242 mM citric acid, and 36 mM trisodium citrate was used as the electrolyte. Potentials used for Cu and In deposition were fixed at −0.2 and −0.76 V (vs Ag/AgCl), respectively. Electric charges of Cu and In deposition were fixed at 0.73 and 0.84 C, respectively: this resulted in the composition ratio of Cu and In (Cu/In) in a Cu and In stacked layer of 1.3. The Cu/In stack as-deposited was then heated at 160 °C for 30 min under Ar flow (200 mL min^{-1}), followed by sulfurization at 560 °C under H_2S flow (5% H_2S in Ar, 200 mL min^{-1}) for 10 min in a glass tube furnace. Thus-obtained $CuInS_2$ films were then etched by immersion in an aqueous KCN solution (10%) for 2 min to remove excess Cu_xS components.

Surface Modification with an In_2S_3 Layer. Surface modification of the prepared $CuInS_2$ film by In_2S_3 layers was performed by the chemical bath deposition (CBD) method. In a typical procedure, the prepared $CuInS_2$ was added to an aqueous solution containing 25 mM $In_2(SO_4)_3$, 0.1 M CH_3CSNH_2 and 0.1 M CH_3COOH; deposition of In_2S_3 was performed at 65 °C for 15 min. Finally, the film was washed with demineralized water. The deposition resulted in the formation of *ca.* 15 nm-thick In_2S_3 layers on the $CuInS_2$ films (labeled In_2S_3/$CuInS_2$). The In_2S_3 layer was also deposited on a fluorine-doped tin oxide (FTO)/glass substrate.

Surface Modification with a CdS Layer. CdS layers on the surfaces of the $CuInS_2$ electrodes were also deposited by CBD. The $CuInS_2$ film was immersed in an aqueous solution containing 12.5 mM $CdSO_4$, 0.22 M H_2NCSNH_2 and 11 M NH_4OH at 60 °C for 7 min. Then the film was washed with demineralized water. The CdS thicknesses were *ca.* 50−60 nm (labeled CdS/$CuInS_2$). The CdS layer was also fabricated on a FTO/glass substrate.

Surface Modification with Pt. Depositon of Pt particles on $CuInS_2$, In_2S_3/$CuInS_2$, and CdS/$CuInS_2$ films was done by photoelectrodeposition using 20 mL of a solution containing 0.1 M Na_2SO_4 and 1 mM H_2PtCl_6 at pH 4. Three electrodes, namely Pt wire, Ag/AgCl and $CuInS_2$-based films as counter, reference and working electrodes, respectively, were inserted into a three-necked cylindric flask with a flat window containing the above-mentioned deposition bath. By illuminating the working electrode with simulated sunlight (AM1.5) using an Asahi Spectra HAL-320 Compact Xenon Light Source, Pt deposition was performed at a potential of −0.1 V for 10 min using a Solartron SI 1280B electrochemical measurement unit. Thus-obtained CdS/$CuInS_2$ and In_2S_3/$CuInS_2$ modified with Pt particles were labeled Pt-CdS/$CuInS_2$ and Pt−In_2S_3/$CuInS_2$, respectively.

Photoelectrochemical Measurements. Photoelectrochemical measurements were performed under N_2 using the same three-electrode setup as that used for the depostion of Pt particles. The electrolyte solution used for PEC water splitting was 0.2 M NaH_2PO_4 (at pH 6). PEC measurements under an electron acceptor (Eu^{3+}) were also performed by using 0.2 M $Eu(NO_3)_3$ solutions with pH adjusted to 4. All of the measurements were conducted by a linear sweep voltamonmetric mode with a negative scan direction at the scan rate of 10 mV s^{-1} under chopped illumination at a frequency of 10 Hz.

Potentials of these PEC measurements that referred to the Ag/AgCl electrode ($E_{Ag/AgCl}$) were converted to those that referred to the reversible hydrogen electrode (E_{RHE}) by using the following equation:

$$E_{RHE} = E_{Ag/AgCl} + 0.059 \times pH + 0.199.$$

The half-cell solar-to-hydrogen efficiency (HC-STH) was determined from the current density-potential (J−V) response of the photocathodes by using the following equation:[18,19]

$$\text{HC-STH}(\%) = J \times (V - V_{H+/H2}) \times 100\%/P$$

where $V_{H+/H2}$ and P are the equilibrium redox potential of hydrogen (0 V vs RHE) and intensity of simulated sunlight (100 mW cm^{-2}), respectively.

Characterizations of Fabricated Photocathodes. Phtotoabsorption properties were examined by using a Hitachi U-4100 UV/vis/NIR spectrophotometer. X-ray photoelectron (XP) spectroscopy was performed by using a Shimadzu AXIS ULTRA X-ray photoelectron spectrometer in monochromated Al Kα ($h\nu$ = 1486.6 eV) radiation. For the surface echting, the sample was bombarded by Ar^+ ions accelerated to 3.5 keV for appropriate durations.

3. RESULTS AND DISCUSSION

Figure 1a shows J−V curves obtained by using Pt-$CuInS_2$, Pt−In_2S_3/$CuInS_2$, and Pt-CdS/$CuInS_2$ electrodes in 0.2 M NaH_2PO_4 at pH 6 under chopped sunlight (AM1.5) illumination. All the photocathodes showed appreciable photocurrents when applying certain bias potentials. Since there were negligible currents observed on the electrodes under

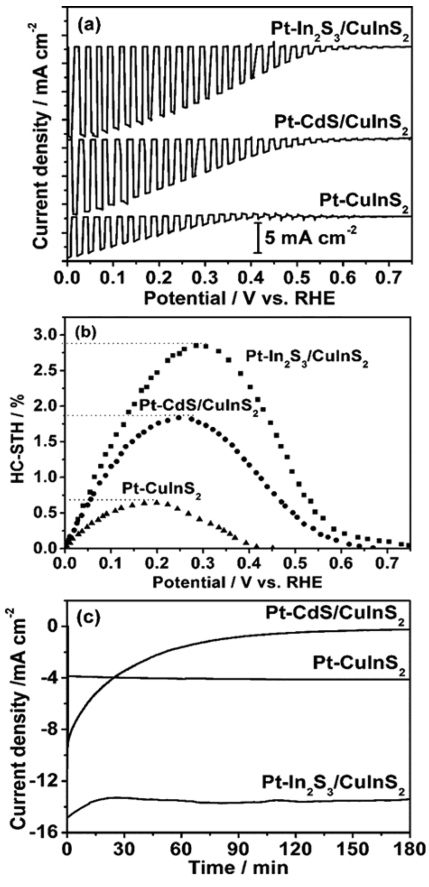

Figure 1. (a) J−V curves, (b) HC-STH spectra, and (c) J−time (J−t) curves of Pt-$CuInS_2$, Pt-CdS/$CuInS_2$, and Pt−In_2S_3/$CuInS_2$ in 0.2 M NaH_2PO_4 (pH 6) under illumination of simulated sunlight (AM 1.5G).

DOI: 10.1021/acsami.5b04634
ACS Appl. Mater. Interfaces 2015, 7, 16086−16092

dark conditions (without photoirradiation), the observed photocurrents were solely from the reduction of H_2O to H_2. As expected from the results reported in the literature,[8,12] the photocurrent density was increased by deposition of CdS and In_2S_3 layers on $CuInS_2$: they gave an appreciable positive shift of photocurrent onset as well as relatively large photocurrent densities in the whole potential regions. These results revealed that formation of a p−n junction via deposition of the n-type layers resulted in a favorable charge transfer due to the formation of a larger built-in field of these p-n semiconductor junctions than that of a p-type $CuInS_2$-electrolyte junction.[20−22] When compared to the Pt-CdS/$CuInS_2$ electrode, the Pt−In_2S_3/$CuInS_2$ electrode showed a positive photocurrent onset potential: when the onset potential was defined as the potential reaching 0.1 mA cm^{-2} of cathodic photocurrent, the onset potentials of Pt−In_2S_3/$CuInS_2$ and Pt-CdS/$CuInS_2$ were 0.72 and 0.59 V (vs RHE), respectively. Regarding the photocurrent density, moreover, Pt−In_2S_3/$CuInS_2$ showed relatively large values, e.g., the value of the Pt−In_2S_3/$CuInS_2$ electrode at the bias voltage of 0 V (vs RHE) was ca. 18 mA cm^{-2} with faradaic efficiency close to 100% (Figure S1), whereas that obtained by the Pt-CdS/$CuInS_2$ electrode was less than 11 mA cm^{-2} at the same potential. As shown in Figure 1b, HC-STH values estimated by the $J-V$ curves reached maximum values of 2.9% (at 0.30 V (vs RHE) and 1.8% (at 0.25 V (vs RHE) for Pt−In_2S_3/$CuInS_2$ and Pt-CdS/$CuInS_2$, respectively. It is noted that the HC-STH of the Pt−In_2S_3/$CuInS_2$ in the present electrolyte is higher compared to our previous report (2%). This was likely due to stabilization of the surface pH of the electrode by buffer species in phosphate electrolyte which promotes more HER activity, as has been reported by Auinger et al.[23] and Kumagai et al.[24]

Time courses of photocurrents of these three electrodes were evaluated at 0 V (vs RHE). As shown in Figure 1c, the Pt−In_2S_3/$CuInS_2$ electrode showed a photocurrent 1.5 times higher than that for the Pt-CdS/$CuInS_2$ electrode in the initial stage of photoirradiation. It is also noted that the Pt−In_2S_3/$CuInS_2$ electrode maintained the constant photocurrent for 180 min, whereas the photocurrent obtained by the Pt-CdS/$CuInS_2$ electrode appreciable decrease: it reached almost zero after the 180 min photoirradiation. The fact that Pt-$CuInS_2$ showed appreciable low but stable photocurrents, the observed decrease in the photocurrent on electrode Pt-CdS/$CuInS_2$ was attributed to be degradation of the surface modified CdS layer.

Figure 2a shows typical transmittance spectra of the In_2S_3 and CdS layers deposited by the CBD technique on glass substrates. Both of the films showed more than 60% transparency in visible and near-infrared regions at wavelengths of more than ca. 500 nm; relatively high transparency of the In_2S_3 film was attributable to the low scattering loss due to its thinner optimum thickness than that of the CdS film (see experimental). At the shorter wavelength region (below ca. 500 nm), appreciable drops in transparencies appeared due to their band gap (E_g) photoexcitation. In order to determine their E_g values, a Tauc plot expressed as the following equation was applied to the transmission spectra.

$$(\alpha h\nu)^n = A(h\nu - E_g)$$

where α is the absorption coefficient, $h\nu$ is the incident photon energy, A is a proportionality constant, and n varies from 0.5 to 2.0 depending on the nature of the optical transition. For the CdS film, a straight line for the $(\alpha h\nu)^2$ (i.e., $n = 2$) plot was obtained, indicating a direct band character of the film (Figure 2b).[25] On the other hand, a straight plot was obtained for the In_2S_3 film by applying $n = 1/2$ to the Tauc plot because of its indirect character, as shown in Figure 2c.[26,27] From intersects of the linear portions of these $(\alpha h\nu)^n$ vs $A(h\nu-E_g)$ curves with the photon energy axis, the E_g values of CdS and In_2S_3 films used in this study were determined to be 2.44 and 2.24 eV, respectively. These values almost correspond to those of bulk compounds of cubic CdS and In_2S_3, respectively. It should be noted that a small shoulder component observed in the plot for the In_2S_3 film suggested presence of different phases such as ß-tetragonal phase.[26]

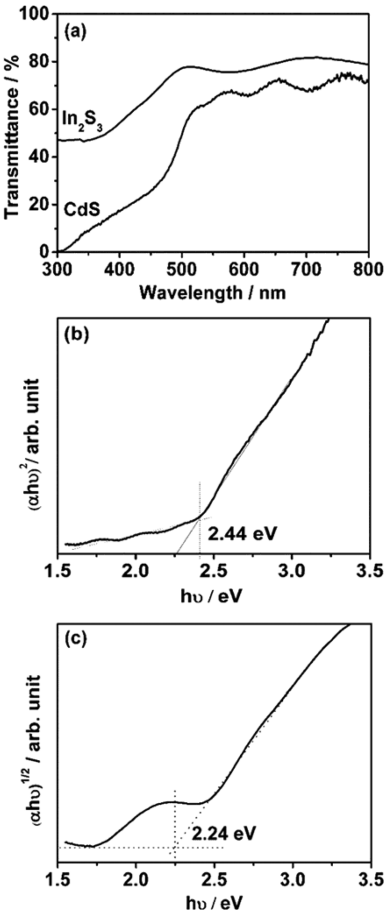

Figure 2. (a) Transmission spectra of In_2S_3 and CdS films on an FTO substrate prepared by chemical bath deposition. (b) Plot of $(\alpha h\nu)^2$ versus $h\nu$ for the optical direct transition of CdS. (c) Plot of $(\alpha h\nu)^{1/2}$ versus $h\nu$ for the indirect transition of In_2S_3.

As discussed in our previous report,[12] one of the probable reasons for the relatively large photocurrent density of the Pt−In_2S_3/$CuInS_2$ electrode compared to that of the Pt-CdS/$CuInS_2$ electrode is better transparency of the In_2S_3 layer than that of the CdS layer. This probable reason is supported by results of the photoabsortion properties of CdS and In_2S_3 films. However, it is not the sole reason for such an appreciable photocurrent improvement of Pt−In_2S_3/$CuInS_2$, and there is no reasonable experimental evidence or explanation for the relatively positive onset potential achieved on the electrode. In order to examine these points, $J-V$ responses of $CuInS_2$, In_2S_3/$CuInS_2$, and CdS/$CuInS_2$ in an 0.2 M $Eu(NO_3)_3$ solution (pH 4) were investigated. Since the standard electrode potential of the Eu^{3+}/Eu^{2+} redox couple (ca. −0.58 V (vs Ag/AgCl)) is much more positive than the flatband potential of CdS (ca.

DOI: 10.1021/acsami.5b04634
ACS Appl. Mater. Interfaces 2015, 7, 16086−16092

−0.94 V(vs Ag/AgCl)),[28,29] moreover, XPS results (see below) suggested that the flatband potential of In_2S_3 would be more negative than that of CdS, the Eu^{3+} ion in the electrolyte should be a good acceptor of photoexcited electrons formed in In_2S_3/$CuInS_2$ and CdS/$CuInS_2$ heterojunctions, i.e., we can solely investigate intrinsic junction properties without considering the required overpotential of water reduction over the surface-loaded Pt particles. As can be seen in this figure (Figure 3), both In_2S_3/$CuInS_2$ and CdS/$CuInS_2$ electrodes gave appreciable photocurrent densities of more than 10 mA cm^{-2}. One of the significant differences between these electrodes is photocurrent onset: onset of the photocurrent of the In_2S_3/$CuInS_2$ junction (ca. 0.17 V vs Ag/AgCl) was observed at a more positive potential than that of the CdS/$CuInS_2$ junction (ca. 0.10 V vs Ag/AgCl), similar to those observed in the above PEC water reduction (see Figure 1). As has been reported in the literature discussing photovoltaics based on the CdS/$CuInS_2$ junction,[30] the CdS-$CuInS_2$ interface is considered to be a "cliff-type" conduction band alignment: the conduction band minimum (CBM) of CdS is deeper than that of $CuInS_2$ (i.e., $\Delta CBM^{CdS\text{-}CIS} < 0$). In such a band alignment, it is known that recombination at the CdS-$CuInS_2$ interface is dominant,[31] i.e., the maximum photovoltage retrieved from the CdS/$CuInS_2$ junction should be affected by such an interface recombination. Thus, positive shifts of onset potentials induced by using the In_2S_3/$CuInS_2$ junction as shown in Figures 1 and 3 should be attributed to induction of favorable modulation at the heterointerface.

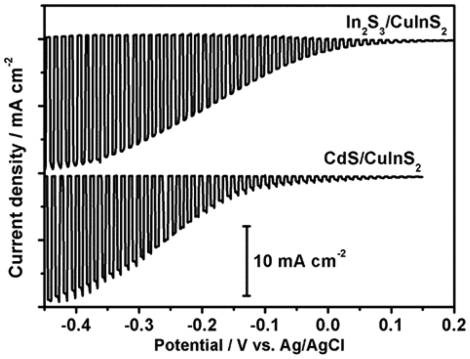

Figure 3. J–V curves of CdS/$CuInS_2$ and In_2S_3/$CuInS_2$ electrodes obtained from an aqueous 0.2 M $Eu(NO_3)_3$ solution (pH 4) under chopped illumination of simulated sunlight (AM1.5).

In order to elucidate the differences in the electric structures of CdS/$CuInS_2$ and In_2S_3/$CuInS_2$ junctions, the valence band maximum (VBM) of each of these heterostructures was determined by XP spectroscopy as reported by Kraut and co-

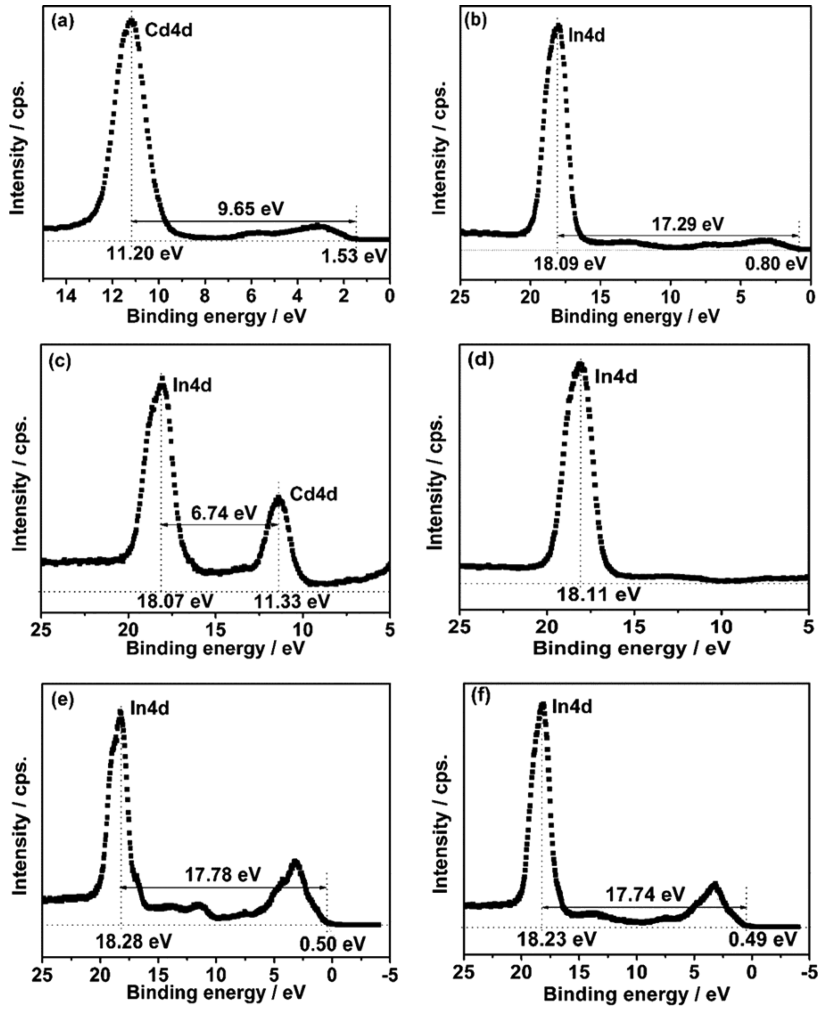

Figure 4. Typical XP spectra of (a, c, e) CdS/$CuInS_2$ and (b, d, f) In_2S_3/$CuInS_2$ heterostructures obtained after Ar^+ ion etching for (a, b) 2 min, (c, d) 25 min, and (e, f) 85 min.

DOI: 10.1021/acsami.5b04634
ACS Appl. Mater. Interfaces 2015, 7, 16086−16092

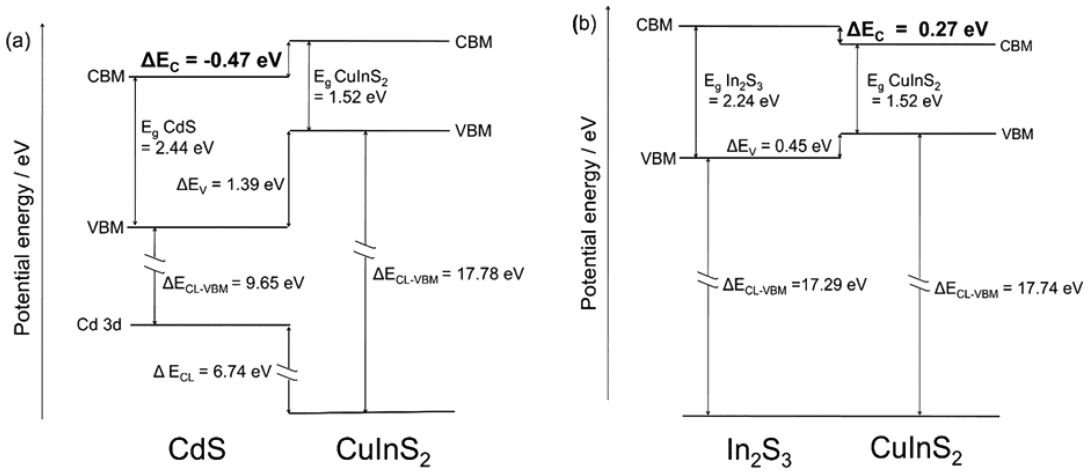

Figure 5. Energy diagrams of (a) $CdS/CuInS_2$ and (b) $In_2S_3/CuInS_2$ heterojunctions estimated from photoabsorption and XP spectroscopy data. The E_g value of $CuInS_2$ was obtained from ref 8.

workers.[32] Figure 4 shows typical XP spectra of $CdS/CuInS_2$ and $In_2S_3/CuInS_2$ samples at a shallow binding energy (BE) level region (<25 eV). Before the measurement, both of the samples were bombarded by Ar^+ within a short duration (2 min) to expose clean CdS and In_2S_3 surfaces, respectively. The $CdS/CuInS_2$ sample showed an intense peak derived from the Cd 4d core level with BE (BE_{Cd}) of 11.20 eV in addition to a broad spectrum at the valence band region. Assuming that the onset BE (1.53 eV) of the valence band spectrum is VBM (VBM_{CdS}), the energy difference between BE_{Cd} and VBM_{CdS} (ΔE_{CdS}) was determined to be 9.65 eV (Figure 4a). When the same analysis was applied to the $In_2S_3/CuInS_2$ sample, BE of the In 4d core level (BE_{In}), VBM of In_2S_3 (VBM_{In2S3}), and their energy difference (ΔE_{In2S3}) were determined to be 18.09, 0.80, and 17.29 eV, respectively (Figure 4b). After the surface of $CdS/CuInS_2$ had been bombarded by Ar^+ for 25 min to be etched to some extent, an In 4d core level peak appeared in addition to the Cd 4d peak (Figure 4c), indicating the observation of the $CdS/CuInS_2$ heterointerface. The difference in these two peaks, defined as $\Delta E_{CL}^{CdS\text{-}CIS}$, was calculated to be 6.74 eV. When further Ar^+ ion etching (for 85 min) was applied to the $CdS/CuInS_2$ sample, the Cd 4d peak disappeared; the XP spectrum showed the surface structure of the bottom $CuInS_2$ layer, as shown in Figure 4e. Based on the result of analysis of the sample without Ar^+ ion etching, BE of the In 4d core level (BE_{In}), VBM of $CuInS_2$ (VBM_{CIS}), and their energy difference (ΔE_{CIS}) of the bottom $CuInS_2$ part in $CdS/CuInS_2$ were calculated to be 18.28, 0.50, and 17.78 eV, respectively. For the $In_2S_3/CuInS_2$ sample, there was no difference in BE_{In} before and after Ar^+ ion etching, indicating no energy differences between the In 4d core levels of both In_2S_3 and $CuInS_2$ layers (i.e., $\Delta E_{CL}^{In2S3\text{-}CIS} = 0$ eV) (Figure 4d). In order to expose the bottom layer of the $In_2S_3/CuInS_2$ sample, Ar^+ ion etching was continued until the intensity of the Cu 2p3/2 peak became constant; BE_{In}, VBM_{CIS}, and ΔE_{CIS} of the bottom $CuInS_2$ part in $In_2S_3/CuInS_2$ were calculated to be 18.23, 0.49, and 17.74 eV, respectively (Figure 4f).

As shown in our previous study, E_g of the present $CuInS_2$ layer is 1.52 eV.[8] Moreover, E_gs of In_2S_3 and CdS films were determined to be 2.24 and 2.44 eV, respectively (see Figure 1). Based on these values and the above parameters obtained by XP spectra, schematic energy diagrams of $In_2S_3/CuInS_2$ and $CdS/CuInS_2$ interfaces are as shown in Figure 5. Significant results of these analyses of electronic structures are differences in conduction band alignments. $\Delta CBM^{CdS\text{-}CIS}$ of the $CdS/CuInS_2$ sample is largely negative (0.47 eV), indicating cliff-type conduction band alignment, which is in agreement with results in the literature.[13,33−35] On the other hand, the conduction band alignment between the In_2S_3 and $CuInS_2$ layers in the $In_2S_3/CuInS_2$ sample ($\Delta CBM^{In2S3\text{-}CIS}$) is slightly positive (0.27 eV), indicating formation of a favorable "notch-type" conduction band alignment for efficient suppression of the interface recombination, similar to the CdS-Cu(In,Ga)Se_2 interface of a highly efficient solar cell.[36] In the case of cliff-type band alignment on $CdS/CuInS_2$, the electrons generated on the CBM of $CuInS_2$ upon illumination will lose some of its energy when transported to CBM of CdS and led to an increase of probability of cross recombination with the holes (majority carrier) at VBM of $CuInS_2$ due to the relatively narrow energy difference between CBM of CdS and VBM of $CuInS_2$ ($CBM^{CdS} - VBM^{CIS} = 1.05$ eV). This interface recombination will be suppressed at the notch-type junction of $In_2S_3/CuInS_2$ since the energy difference between CBM of In_2S_3 and VBM of $CuInS_2$ is sufficiently large ($CBM^{In2S3} - VBM^{CIS} = 1.79$ eV), so that the charge can be separated and transported more efficiently. Thus, the difference in these energetic structures should be one of the main causes of the different photocurrent onsets of $In_2S_3/CuInS_2$ and $CdS/CuInS_2$ junctions.

As discussed above, the current density of the best $Pt-In_2S_3/CuInS_2$ electrode shown in Figure 1 was 16.4 mA cm^{-2} (at 0 V vs RHE) obtained by applying a potential of 0.72 V from its onset The current density of the electrode system composed of the same $In_2S_3/CuInS_2$ heterojunction in the Eu^{3+}-containing electrolyte (see Figure 3) by applying a similar potential from its onset reached close to 20 mA cm^{-2}. The difference between the photocurrents in these two systems is likely to be due to the presence of bottlenecks to suppress efficient electron transfer from the $In_2S_3/CuInS_2$ junction toward the Pt catalyst. Based on the above XP spectroscopy results, CBM of the In_2S_3 layer in the present $In_2S_3/CuInS_2$ junction was highly negative. Since the work function of Pt was relatively large (5.65 eV),[37] there would be possible formation of a Schottky-type potential barrier that inhibits electron transfer. Thus, a metal catalyst having a relatively small work function would be a better candidate to reduce such a barrier height. For the further improvement of the PEC water splitting property of the

DOI: 10.1021/acsami.5b04634
ACS Appl. Mater. Interfaces 2015, 7, 16086−16092

photocathode based on the $In_2S_3/CuInS_2$ junction, studies along this line is underway.

4. CONCLUSION

For PEC water reduction under simulated sunlight radiation in an aqueous NaH_2PO_4 solution (pH 6), $Pt-In_2S_3/CuInS_2$ showed a larger photocurrent density and a more positive onset potential than those of Pt-CdS/$CuInS_2$. PEC analysis in an aqueous solution containing an electron acceptor (Eu^{3+}) revealed the formation of a better $In_2S_3/CuInS_2$ heterojunction than the CdS/$CuInS_2$ heterojunction. Evaluation of the valence band offsets of $In_2S_3/CuInS_2$ and CdS/$CuInS_2$ using photoabsorption spectroscopy and XP spectroscopy revealed a favorable notch-type positive conduction band offset in the $In_2S_3/CuInS_2$ heterojunction, whereas the CdS/$CuInS_2$ junction had an unfavorable cliff-type negative offset, leading to enhancement of the interface carrier recombination photocathode of $In_2S_3/CuInS_2$. For further improvement of the PEC water reduction property, therefore, there is room for improvements of junction properties by appropriate engineering of band structures as well as development of efficient surface-loaded catalysts for hydrogen production.

■ ASSOCIATED CONTENT

Supporting Information

Time courses of H_2 evolution over the $Pt-In_2S_3/CuInS_2$ photocathode and half of the electrons passing through the outer circuit ($e^-/2$) measured at 0.2 M NaH_2PO_4 (pH 6) at 0 V (vs RHE) under simulated sunlight (AM 1.5G) radiation. The Supporting Information is available free of charge on the ACS Publications website at DOI: 10.1021/acsami.5b04634.

■ AUTHOR INFORMATION

Corresponding Author

*E-mail: sikeda@chem.es.osaka-u.ac.jp.

Notes

The authors declare no competing financial interest.

■ ACKNOWLEDGMENTS

This work was supported by a Grant-in-Aid for Scientific Research on Innovative Areas (All Nippon Artificial Photosynthesis Project for Living Earth) and a Grant-in-Aid for Scientific Research (B) from MEXT Japan. This work was also carried out as a part of the A-step feasibility study program from JST Japan. Financial support for Gunawan by DGHE (270/E4.4/K/2012), Ministry of Education and Culture of Republic of Indonesia, is acknowledged.

■ REFERENCES

(1) Fujishima, A.; Honda, K. Electrochemical Photolysis of Water at a Semiconductor Electrode. *Nature* **1972**, *238*, 37−38.

(2) Domen, K.; Kondo, J. N.; Hara, M.; Takata, T. Photo- and Mechano-Catalytic Overall Water Splitting Reactions to Form Hydrogen and Oxygen on Heterogeneous Catalysts Bull. *Bull. Chem. Soc. Jpn.* **2000**, *73*, 1307−1331.

(3) Sato, J.; Saito, N.; Yamada, Y.; Maeda, K.; Takata, T.; Kondo, J. N.; Hara, M.; Kobayashi, H.; Domen, K.; Inoue, Y. RuO_2-Loaded ß-Ge_3N_4 as a Non-Oxide Photocatalyst for Overall Water Splitting. *J. Am. Chem. Soc.* **2005**, *127*, 4150−5151.

(4) Maeda, K.; Teramura, K.; Lu, D.; Takata, T.; Saito, N.; Inoue, Y.; Domen, K. *Nature* **2006**, *440*, 295.

(5) Maeda, K.; Domen, K. New Non-Oxide Photocatalysts Designed for Overall Water Splitting under Visible Light. *J. Phys. Chem. C* **2007**, *111*, 7851−7861.

(6) Osterloh, F. E. Inorganic Materials as Catalysts for Photochemical Splitting of Water. *Chem. Mater.* **2008**, *20*, 35−54.

(7) Yokoyama, D.; Minegishi, T.; Maeda, K.; Katayama, M.; Kubota, J.; Yamada, A.; Konagai, M.; Domen, K. Photoelectrochemical Water Splitting Using a Cu(In,Ga)Se_2 Thin Film. *Electrochem. Commun.* **2010**, *12*, 851−853.

(8) Ikeda, S.; Nakamura, T.; Lee, S. M.; Yagi, T.; Harada, T.; Minegishi, T.; Matsumura, M. Photoreduction of Water by Using Modified $CuInS_2$ Electrodes. *ChemSusChem* **2011**, *4*, 262−268.

(9) Kim, J.; Minegishi, T.; Kubota, J.; Domen, K. Enhanced Photoelectrochemical Properties of $CuGa_3Se_5$ Thin Films for Water Splitting by the Hydrogen Mediated Co-evaporation. *Energy Environ. Sci.* **2012**, *5*, 6368−6374.

(10) Djellal, L.; Bellal, B.; Trari, M. Physical, Photoelectrochemical Properties of $CuIn_3Se_5$ and Relevance for Hydrogen Production Mater. *Mater. Chem. Phys.* **2012**, *137*, 340−345.

(11) Ikeda, S.; Nonogaki, M.; Septina, W.; Gunawan, G.; Harada, T.; Matsumura, M. Fabrication of $CuInS_2$ and Cu(In,Ga)S_2 Thin films by a Facile Spray Pyrolysis and Their Photovoltaic and Photoelectrochemical Properties Catal. *Catal. Sci. Technol.* **2013**, *3*, 1849−1854.

(12) Gunawan; Septina, W.; Ikeda, S.; Harada, T.; Minegishi, T.; Domen, K.; Matsumura, M. Platinum and Indium Sulfide-Modified $CuInS_2$ as Efficient Photocathodes for Photoelectrochemical Water Splitting. *Chem. Commun.* **2014**, *50*, 8941−8943.

(13) Septina, W.; Gunawan; Ikeda, S.; Harada, T.; Higashi, M.; Abe, R.; Matsumura, M. Photosplitting of Water from Wide-Gap Cu(In,Ga)S_2 Thin Films Modified with a CdS Layer and Pt Nanoparticles for a High-Onset-Potential Photocathode. *J. Phys. Chem. C* **2015**, *119*, 8576−8583.

(14) Moriya, M.; Minegishi, T.; Kumagai, H.; Katayama, M.; Kubota, J.; Domen, K. Stable Hydrogen Evolution from CdS-Modified $CuGaSe_2$ Photoelectrode under Visible-Light Irradiation. *J. Am. Chem. Soc.* **2013**, *135*, 3733−3735.

(15) Yokoyama, D.; Minegishi, T.; Jimbo, K.; Hisatomi, T.; Ma, G.; Katayama, M.; Kubota, J.; Katagiri, H.; Domen, K. H_2 Evolution from Water on Modified Cu_2ZnSnS_4 Photoelectrode under Solar Light. *Appl. Phys. Express* **2010**, *3*, 101202.

(16) Ma, G.; Minegishi, T.; Yokohama, D.; Kubota, J.; Domen, K. Photoelectrochemical Hydrogen Production on Cu_2ZnSnS_4/Mo-mesh Thin-Film Electrodes Prepared by Electroplating. *Chem. Phys. Lett.* **2011**, *501*, 619−622.

(17) Rovelli, L.; Tilley, S. D.; Sivula, K. Optimization and Stabilization of Electrodeposited Cu_2ZnSnS_4 Photocathodes for Solar Water Reduction. *ACS Appl. Mater. Interfaces* **2013**, *5*, 8018−8024.

(18) Zhang, L.; Minegishi, T.; Nakabayashi, M.; Suzuki, Y.; Seki, K.; Shibata, N.; Kubota, J.; Domen, K. Durable Hydrogen Evolution from Water Driven by Sunlight Using (Ag,Cu)$GaSe_2$ Photocathodes Modified with CdS and $CuGa_3Se_5$. *Chem. Sci.* **2015**, *6*, 894−901.

(19) Zhao, J.; Minegishi, T.; Zhang, L.; Zhong, M.; Gunawan; Nakabayashi, M.; Ma, G.; Hisatomi, T.; Katayama, M.; Ikeda, S.; Shibata, N.; Yamada, T.; Domen, K. Enhancement of Solar Hydrogen Evolution from Water by Surface Modification with CdS and TiO_2 on Porous $CuInS_2$ Photocathodes Prepared by an Electrodeposition-Sulfurization Method Angew. Chem. *Angew. Chem., Int. Ed.* **2014**, *53*, 11808−11812.

(20) Malizia, M.; Seger, B.; Chorkendorff, I.; Vesborg, P. C. Formation of a p−n Heterojunction on GaP Photocathodes for H_2 Production Providing an Open-Circuit Voltage of 710 mV. *J. Mater. Chem. A* **2014**, *2*, 6847−6853.

(21) Ji, L.; McDaniel, M. D.; Wang, S.; Posadas, A. B.; Li, X.; Huang, H.; Lee, J. C.; Demkov, A. D.; Bard, A. J.; Ekerdt, J. G.; Yu, E. T. Y. A Silicon-Based Photocathode for Water Reduction with an Epitaxial $SrTiO_3$ Protection Layer and a Nanostructured Catalyst. *Nat. Nanotechnol.* **2015**, *10*, 84−90.

DOI: 10.1021/acsami.5b04634
ACS Appl. Mater. Interfaces 2015, 7, 16086−16092

(22) Liu, R.; Zheng, Z.; Spurgeon, J.; Yang, X. Enhanced Photoelectrochemical Water-Splitting Performance of Semiconductors by Surface Passivation Layers. *Energy Environ. Sci.* **2014**, *7*, 2504−2517.
(23) Auinger, M.; Katsounaros, I.; Meier, J. C.; Klemm, S. O.; Biedermann, P. U.; Topalov, A. A.; Rohwerder, M.; Mayrhofer, K. J. Near-Surface Ion Distribution and Buffer Effects During Electrochemical Reactions. *Phys. Chem. Chem. Phys.* **2011**, *13* (36), 16384−16394.
(24) Kumagai, H.; Minegishi, T.; Sato, N.; Yamada, T.; Kubota, J.; Domen, K. Efficient Solar Hydrogen Production from Neutral Electrolytes Using Surface-Modified Cu(In,Ga)Se_2 Photocathodes. *J. Mater. Chem. A* **2015**, *3*, 8300−8307.
(25) Kim, D. J.; Yu, Y. M.; Lee, J. W.; Choi, Y. D. Investigation of Energy Band Gap and Optical Properties of Cubic CdS Epilayers. *Appl. Surf. Sci.* **2008**, *254*, 7522−7526.
(26) Sandoval-Paz, M. G.; Sotelo-Lerma, M.; Valenzuela-Jauregui, J. J.; Flores-Acosta, M.; Ramırez-Bon, R. Structural and Optical Studies on Thermal-Annealed In_2S_3 Films Prepared by the Chemical Bath Deposition Technique. *Thin Solid Films* **2005**, *472*, 5−10.
(27) Choe, S. H.; Bang, T. H.; Kim, N. O.; Kim, H. G.; Lee, C. I.; Jin, M. S.; Oh, S. K.; Kim, W. T. Optical Properties of β-In_2S_3 and β-In_2S_3:Co^{2+} Single Crystals . *Semicond. Sci. Technol.* **2001**, *16*, 98−102.
(28) Scragg, J. J.; Dale, P. J.; Peter, L. M.; Zoppi, G.; Forbes, I. New Routes to Sustainable Photovoltaics: Evaluation of Cu_2ZnSnS_4 as an Alternative Absorber Material. *Phys. Status Solidi B* **2008**, *245*, 1772−1778.
(29) Matsumura, M.; Uchihara, T.; Hanafusa, K.; Tsubomura, H. Interfacial Band Structure of Platinum-Loaded CdS Powder and its Correlation with the Photocatalytic Activity. *J. Electrochem. Soc.* **1989**, *136*, 1704−1709.
(30) Siebentritt, S. Wide Gap Chalcopyrites. *Thin Solid Films* **2002**, *403−304*, 1−8.
(31) Konovalov, I. Material Requirements for CIS Solar Cells. *Thin Solid Films* **2004**, *451−452*, 413−419.
(32) Kraut, E. A.; Grant, R. W.; Waldrop, J. R.; Kowalczyk, S. P. Precise Determination of the Valence-Band Edge in X-Ray Photoemission Spectra: Application to Measurement of Semiconductor Interface Potentials. *Phys. Rev. Lett.* **1980**, *44*, 1620−1623.
(33) Scheer, R.; Walter, T.; Schock, H. W.; Fearheiley, M. L.; Lewerenz, H. J. $CuInS_2$ Based Thin Film Solar Cell with 10.2% Efficiency. *Appl. Phys. Lett.* **1993**, *63*, 3294−3296.
(34) Johnson, B.; Korte, L.; Lussky, T.; Klaer, J.; Lauermann, I. $CuInS_2$-CdS Heterojunction Valence Band Offset Measured with Near-UV Constant Final State Yield Spectroscopy. *J. Appl. Phys.* **2009**, *106*, 073712.
(35) Hashimoto, Y.; Takeuchi, K.; Ito, K. Band Alignment at CdS/$CuInS_2$ Heterojunction. *Appl. Phys. Lett.* **1995**, *67*, 980−982.
(36) Contreras, M. A.; Egaas, B.; Ramanathan, K.; Hiltner, J.; Swartzlander, A.; Hasoon, F.; Noufi, R. Progress Toward 20% Efficiency in Cu(In,Ga)Se_2 Polycrystalline Thin-Film Solar Cells. *Prog. Photovoltaics* **1999**, *7*, 311−316.
(37) Michaelson, H. B. The Work Function of The Elements and Its Periodicity. *J. Appl. Phys.* **1977**, *48*, 4729−4733.

DOI: 10.1021/acsami.5b04634
ACS Appl. Mater. Interfaces 2015, 7, 16086−16092